Bioorganic & Medicinal Chemistry 16 (2008) 6436–6447

Contents lists available at ScienceDirect

Bioorganic & Medicinal Chemistry

journal homepage: www.elsevier.com/locate/bmc

Aroyl hydrazones of 2-phenylindole-3-carbaldehydes as novel antimitotic agents

Susanne Vogel [a], Doris Kaufmann [a], Michaela Pojarová [a], Christine Müller [a], Tobias Pfaller [a], Sybille Kühne [b], Patrick J. Bednarski [b], Erwin von Angerer [a,*]

[a] Institut für Pharmazie, Universität Regensburg, D-93040 Regensburg, Germany
[b] Institut für Pharmazie, Universität Greifswald, F.-L.-Jahnstr. 17, D-17489 Greifswald, Germany

ARTICLE INFO

Article history:
Received 22 August 2007
Revised 25 April 2008
Accepted 30 April 2008
Available online 3 May 2008

Keywords:
Phenylindoles
Aroyl hydrazones
Breast cancer cells
Glioblastoma cells
Cell cycle arrest
Apoptosis

ABSTRACT

Cell cycle arrest of malignant cells is an important option for cancer treatment. In this study, we modified the structure of antimitotic 2-phenylindole-3-carbaldehydes by condensation with hydrazides of various benzoic and pyridine carboxylic acids. The resulting hydrazones inhibited the growth of MDA-MB 231 and MCF-7 breast cancer cells with IC_{50} values of 20–30 nM for the most potent derivatives. These 2-phenylindole derivatives also exerted an inhibitory effect on the growth of both proliferating and resting U-373 MG glioblastoma cells. Though the hydrazones exhibited similar structure–activity relationships as the aldehydes, they did not inhibit tubulin polymerization as the aldehydes but were capable of blocking the cell cycle in G_2/M phase. The cell cycle arrest was accompanied by apoptosis as demonstrated by the activation of caspase-3. Since these 2-phenylindole-based hydrazones display no structural similarity with other antitumor drugs they are interesting candidates for further development.

1. Introduction

In previous studies, the 2-phenylindole skeleton has proved to be a versatile structure for the development of compounds with antiproliferative activity against breast cancer cells. Depending on the type and position of the substituents the 2-phenylindoles inhibit the growth of tumor cells by different mechanisms. In our first studies, we synthesized a variety of 2-phenylindoles that acted as estrogen antagonists and inhibited the growth of estrogen-sensitive breast cancer cells by a total estrogen receptor blockade.[1,2] A similar inhibitory effect can be achieved by the inhibition of the enzyme estrone sulfatase by sulfamoyloxy-substituted 2-phenylindoles.[3,4] This enzyme catalyzes the conversion of estrogen sulfates to the free estrogens which are essential for maintaining the growth of hormone-dependent mammary tumors.

More recently, we showed that 2-phenylindoles which carry an aldehyde function in 3-position (**1**, Fig. 1) bind to tubulin and inhibit tubulin polymerization.[5,6] This action blocks the cell cycle in G_2/M phase and gives rise to an antimitotic effect. Unfortunately, these 2-phenylindole derivatives were inactive in vivo probably due to the presence of the metabolically unstable aldehyde group. In order to overcome this problem the aldehyde function was modified by condensation with malononitrile to give the corresponding methylene propanedinitriles **2** (Fig. 1).[7] These derivatives have retained their antimitotic activity but have lost their ability of inhib-

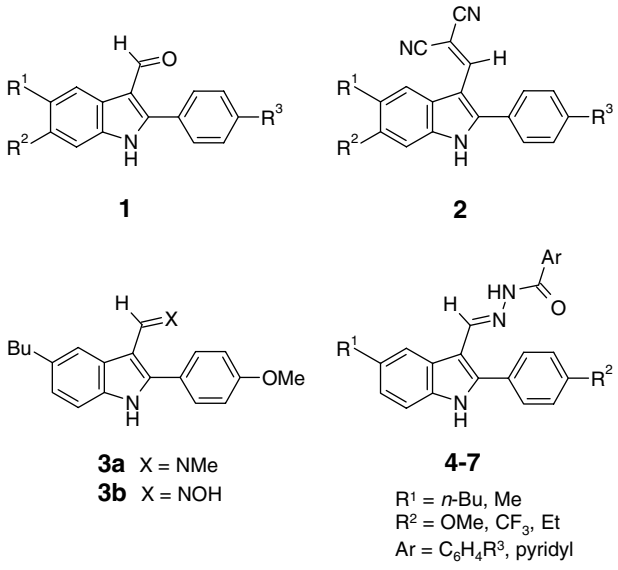

Figure 1. Chemical structures of 2-phenylindole-3-carbaldehydes **1** and analogues **2–7** with antimitotic activity.

* Corresponding author. Tel.: +49 (0) 941 9434821; fax: +49 (0) 941 9434820.
E-mail address: erwin.von-angerer@chemie.uni-regensburg.de (E.von Angerer).

0968-0896/$ - see front matter © 2008 Elsevier Ltd. All rights reserved.
doi:10.1016/j.bmc.2008.04.071

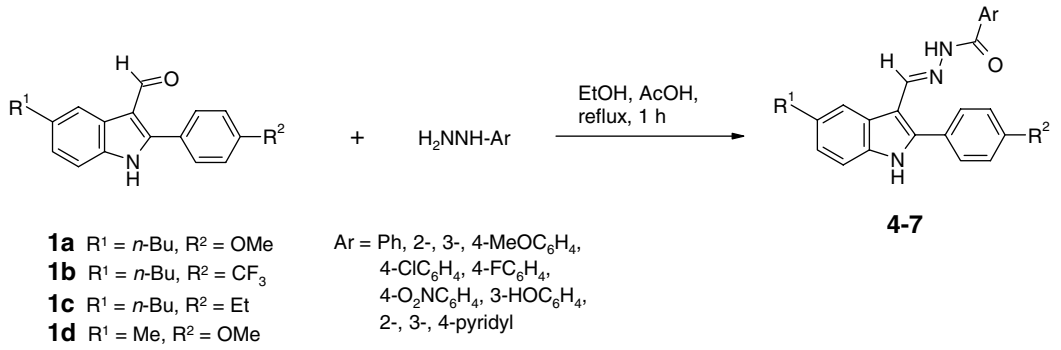

Figure 2. Synthesis of aromatic carboxylic acid [(2-phenylindol-3-yl)methylene]hydrazides **4–7**.

iting tubulin polymerization. Preliminary investigations showed that they are active in vivo and inhibit the growth of MXT mouse mammary tumors.[7] A careful analysis of the biological effects of these agents revealed that they might act by two competing mechanisms which both result in an inhibition of cell growth. Both modes of action involve a cell cycle arrest in G_2/M phase and the induction of apoptosis. In order to get a deeper insight into these processes, other derivatives of 2-phenylindole-3-carbaldehyde were synthesized for more extended studies. Besides the condensation reactions with C–H-acidic compounds such as malononitrile, reactions with amino compounds were considered as appropriate modifications.

In preliminary investigations, we converted some of the aldehydes to imines, for example, **3a** (Fig. 1) and oximes such as **3b**.[6] Derivative **3a** proved to be only a prodrug of **1a** (Fig. 2), whereas **3b** was stable and showed strong antimitotic activity. These results prompted us to synthesize a number of hydrazones that derive from various aromatic carboxylic acid hydrazides. These compounds were studied for their stability to hydrolysis and for their antiproliferative activities in two different human breast cancer cell lines (MDA-MB 231, MCF-7), in the human U-373 MG glioblastoma cell line, and against human HL-60 leukemia cells. Our experience from previous investigations suggested that these agents interfere with the cell cycle either by inhibition of tubulin polymerization or by targeting other processes involved in cell cycle progression. Therefore, assays on tubulin polymerization and flow-cytometric analyses were performed. Also, the activation of caspase-3 involved in the apoptotic pathway to cell death was determined.

2. Results and discussion

2.1. Chemistry

In previous investigations, we elaborated the most favorable substitution pattern of the starting 2-phenylindole-3-carbaldehydes **1** in respect to antimitotic activity.[6] The structure–activity relationships in this series of compounds exhibited a close analogy to those of the corresponding methylene propanedinitriles **2**. The most favorable substitution pattern was provided by linear alkyl chains of 4–6 carbon atoms in 5-position of the indole and a small lipophilic group in *para*-position of the 2-phenyl ring. In the present study, we kept the 5-*n*-butyl group in the indole moiety as the most favorable substituent constant and modified only the *para*-substituent in the phenyl ring slightly (OMe, CF_3, and Et). For structure–activity analyses, we replaced the butyl group in one particular derivative by a methyl substituent (**5d**).

The main variations concerned the aryl group in the hydrazide component. Both a (un)substituted phenyl ring and the three isomeric pyridine rings were employed. The conversion of the aldehydes **1a–d** to the corresponding aroyl hydrazones **4–7** was readily accomplished by the reaction with the respective carboxylic acid hydrazides (Fig. 2). The C=N double bond can give rise to the formation of *E*/*Z* isomers. The dominating isomer possesses *E*-configuration and was often isolated as the only form. By the structural modifications of the carbonyl group the physico-chemical properties of the indole core and the electronic character of the α-carbon atom in 3-position remained unchanged, whereas the structure of the whole molecule was altered considerably by the aroyl hydrazone fragment. Thus, these molecules have to be considered as completely new entities rather than simple derivatives of the parent aldehydes.

An important aspect in the biological investigations is the stability of the hydrazone function toward hydrolysis. Thus, we checked the stability of some of the hydrazones during prolonged heating in aqueous solution by HPLC. Derivatives **4a** and **6a** showed no hydrolysis or other degradation after heating at 70 °C for 48 h. This result, however, does not exclude an enzymatic cleavage of the C=N bond in a biological system. The observed differences between the aldehydes and the corresponding hydrazones in various assays confirm the stability of the hydrazone function toward hydrolysis at least under in vitro conditions.

2.2. Antiproliferative activity

All of the compounds synthesized were first evaluated for antiproliferative activity using hormone-independent human MDA-MB 231 breast cancer cells in a microplate assay. In this assay, cell growth was determined by crystal violet staining of viable cells that were harvested in the log phase after 4 days of incubation (Fig. 3B). As reference compounds the four starting aldehydes (**1a–d**), the oxime **3b**, and the established anticancer drug vincristine were used. First, the benzoyl hydrazones **4** with various substituents at the phenyl ring were studied. All of the hydrazones inhibited the growth of MDA-MB 231 cells, but there was a significant difference between the derivatives with a methoxy group in the phenyl moiety of the 2-phenylindole and those carrying a trifluoromethyl group as the substituent (Table 1). The latter compounds were much less active than the corresponding methoxy derivatives which exhibited IC_{50} values between 19 and 115 nM. In the methoxy series, no strong influence of the substituents in the benzoyl group could be detected (Fig. 3A). Obviously, both nature and position of these phenyl substituents are of minor importance in respect to the antiproliferative potency of the hydrazones, except for the combination of a nitro group in the benzoyl fragment and a trifluoromethyl group at the 2-phenyl ring (**4k**), which abolished most of the activity.

The positive results obtained with the benzoyl hydrazones prompted us to replace the phenyl group by a pyridine ring to

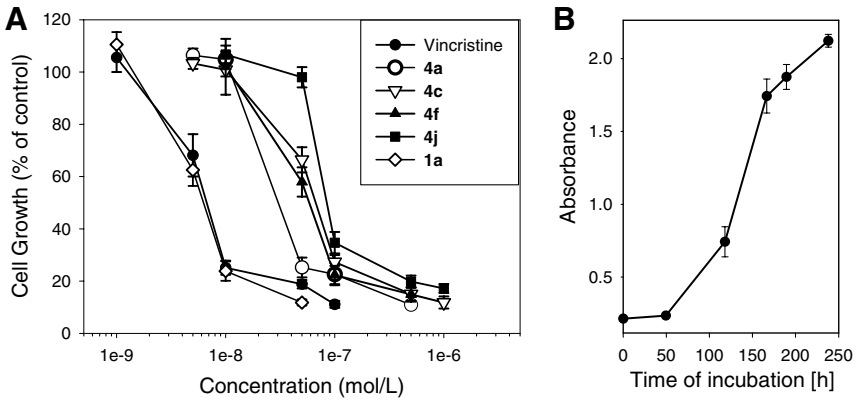

Figure 3. Inhibitory effects of benzoic acid [(2-phenylindol-3-yl)methylene]hydrazides **4** with different benzoyl substituents on the growth of MDA-MB 231 breast cancer cells (A). Inhibition of cell growth was determined after incubation for 4 days and subsequent crystal violet staining of viable cells. Vincristine (Vin) and the parent aldehyde **1a** were used as reference drugs. The growth of untreated cells is shown on (B).

Table 1
Antiproliferative activities of 2-phenylindole-3-carbaldehyde benzoylhydrazones **4** and reference compounds **1a**, **1b**, **3b**, and vincristine

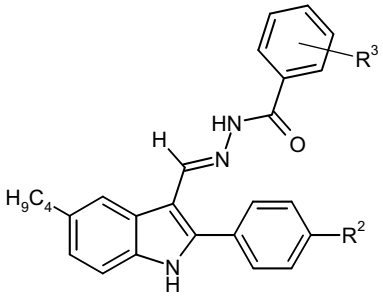

Compound	R^2	R^3	MDA-MB 231[a] IC_{50} (nM)	MCF-7[b] IC_{50} (nM)
1a[c]	OMe		6.7	22
1b[c]	CF_3		33	66
3b[c]	OMe		40	212
4a	OMe	H	32	130
4b	CF_3	H	300	460
4c	OMe	4-Cl	90	220
4d	CF_3	4-Cl	329	1062
4e	OMe	4-F	19	84
4f	OMe	4-Ome	61	226
4g	CF_3	4-Ome	284	618
4h	OMe	3-Ome	55	n.d.[d]
4i	OMe	2-Ome	21	71
4j	OMe	4-NO_2	115	312
4k	CF_3	4-NO_2	2035	6335
4l	OMe	3-OH	30	n.d.
Vincristine			6	2

[a] Inhibition of cell growth determined after incubation for 4 days and subsequent crystal violet staining of viable cells. Mean values of two independent experiments with 16–24 replicates, SD are generally less than 25%.
[b] Analogous experiment as described for MDA-MB 231 cells with one exception: the incubation period was 5 days.
[c] For structures see Figure 1.
[d] Not determined.

avoid additional steric effects by substituents. All three regioisomers **5a**, **6a**, and **7a** with a methoxy group at phenyl ring proved to be potent inhibitors of cell proliferation with IC_{50} values of about 30 nM (Table 2). This value is only fivefold higher than that of the established anticancer drug vincristine (IC_{50}, 6 nM). A minor decrease in activity was noticed when the methoxy group had been replaced by ethyl or trifluoromethyl except for **7b** which is characterized by a considerably reduced potency. The importance of the butyl group in the indole part is underlined by the dramatic decrease in potency upon replacement of this group by a methyl group (**5d**). This effect was similar as in the aldehyde series (**1a** vs **1d**).

In parallel to the investigations with MDA-MB 231 cells, all hydrazones were also tested for antiproliferative activity against estrogen-sensitive MCF-7 breast cancer cells. Generally, the hydrazones were less active against MCF-7 cells than against MDA-MB 231 cells. In the benzoyl hydrazone series (**4**), the IC_{50} values in the latter cell line were lower by a factor of about 2–4 (Table 1), while the difference in the pyridine series was less pronounced (Table 2). This difference between the two cell lines was also observed for the parent aldehydes **1a–d** and the oxime **3b**. A similar variability in sensitivity between these two cell lines was also observed for mitoxantrone.[8] An additional mode of action that involves the estrogen receptor, present in MCF-7 cells, would increase rather than decrease the inhibitory effects of the compounds tested in these cells. Owing to the chemical structures of the compounds, a binding affinity for the estrogen receptor appears to be unlikely. The comparison of the inhibitory effects of the hydrazones with those of the corresponding 2-phenylindole-3-carbaldehydes **1a–d** revealed that the latter are more active by a factor of 3–17.

The high potency of some of the hydrazones makes them interesting candidates for the treatment of malignant tumors from other tissues such as the brain. Therefore, another set of experiments was initiated in which two of the hydrazones were tested for growth inhibition of human U-373 MG human glioblastoma cells. In these experiments, the effect of treatment at various dose levels was monitored over time. Similar as in the assays with breast cancer cells a strong inhibition of cell proliferation was observed. Compound **4e** at a concentration of 50 nM suppressed cell growth already after 72 h completely (Fig. 4A). A similar result was obtained with the pyridine derivative **6a**, which showed already good activity at 10 nM but the SDs for this concentration were rather high (Fig. 4B).

A major problem in cancer treatment arises from the fact that quiescent tumor cells do not respond to the majority of cytostatic agents. A way to mimic the situation of a solid tumor in which most of the cells do not proliferate in vitro is the use of confluent cell cultures. Both compounds, **4e** and **6a**, inhibited the growth of confluent U-373 MG cells after 100 h of incubation at 200 nM (Fig. 5). The established antitumor drug paclitaxel was inactive and showed the same dose–response curve as untreated control cells. Rotenone, an ubiquinone reductase inhibitor that blocks ATP synthesis, was used as positive control. It killed most of the cells within 72 h of treatment.

Table 2
Antiproliferative activities of 2-phenylindole-3-carbaldehyde pyridoylhydrazones **5–7**

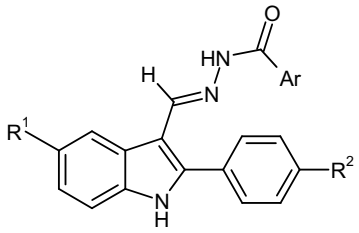

Compound	Ar	R^1	R^2	MDA-MB 231[a] IC_{50} (nM)	MCF-7[b] IC_{50} (nM)
1c		*n*-Bu	Et	27	58
1d		Me	OMe	86	140
5a	4-Pyridyl	*n*-Bu	OMe	29	69
5b	4-Pyridyl	*n*-Bu	CF_3	94	100
5c	4-Pyridyl	*n*-Bu	Et	80	150
5d	4-Pyridyl	Me	OMe	290	200
6a	3-Pyridyl	*n*-Bu	OMe	35	75
6b	3-Pyridyl	*n*-Bu	CF_3	97	260
6c	3-Pyridyl	*n*-Bu	Et	53	100
7a	2-Pyridyl	*n*-Bu	OMe	34	160
7b	2-Pyridyl	*n*-Bu	CF_3	260	310
Vincristine				6	2

[a] Inhibition of cell growth determined after incubation for 4 days and subsequent crystal violet staining of viable cells. Mean values of two independent experiments with 16–24 replicates, SD are generally less than 25%.
[b] Analogous experiment as described for MDA-MB 231 cells with one exception: the incubation period was 5 days.

2.3. Cell cycle arrest in G_2/M-phase

Previous studies with 2-phenylindole-3-carbaldehydes **1** have shown that these aldehydes exert their cytotoxic effects through inhibition of tubulin polymerization and cell cycle arrest in G_2/M-phase. The structural analogy of the hydrazones and the aldehydes suggested a similar mode of action. Therefore, we studied the effect of the most active hydrazones (**4a**) on the cell cycle in comparison with vincristine, a vinca alkaloid that acts by inhibition of tubulin polymerization. The cell cycle dependent DNA content was determined by flow cytometry using propidium iodide in permeabilized cells. Treatment of the cells with **4a** led to a decrease of the peak for cells in the G_1/G_0 phase and the parallel increase of the number of cells in G_2/M phase due to the blockade of the cell cycle in G_2/M phase (Fig. 6). This change in cell cycle distribution was accompanied by the appearance of a significant fraction of cells with a DNA content lower than that in G_1/G_0 cells (sub-G_1 fraction). A cell cycle arrest similar to that of vincristine (0.1 μM) was reached at a concentration of 0.5 μM of the hydrazone. The comparison with the corresponding aldehyde **1a** showed that the potency had dropped by one order of magnitude upon the conversion to the hydrazone (Fig. 7A). Similar activity was observed for the nicotinoyl hydrazone **6a**, whereas the corresponding trifluoromethyl derivative **6b** was somewhat less potent (Fig. 7B)

The cell cycle arrest can be rationalized by the interference with the formation of microtubules. Thus, two representative hydrazones (**4a** and **6a)** were tested for their effects on tubulin polymerization in a microplate assay. The progression of tubulin polymerization was measured turbidimetrically at 350 nm over 28 min after the temperature had been raised from 2 to 37 °C. At a concentration of 5 μM, both hydrazones displayed identical curves slightly above the control curve (Fig. 8). In this assay, the reference drug colchicine (5 μM) strongly inhibited tubulin polymerization whereas paclitaxel (2 μM) rapidly converted tubulin to microtubules. Obviously, the hydrazones did not interfere with the process of tubulin polymerization.

This finding was confirmed by the images obtained by confocal fluorescence microscopy of U-87 glioma cells treated with **4e** (50 nM). Untreated U-87 MG human glioma cells display the normal distribution of microtubules (Fig. 9A). In dividing cells their functional role can be demonstrated (Fig. 9A-a, -b, and -c). Treatment of cells with 10 nM vincristine gave rise to a disruption of the microtubule network and a loss of its function in the mitotic process (Fig. 9B). When the cells were treated with the hydrazone **4e** (50 nM), the microtubule network was rather similar to that of

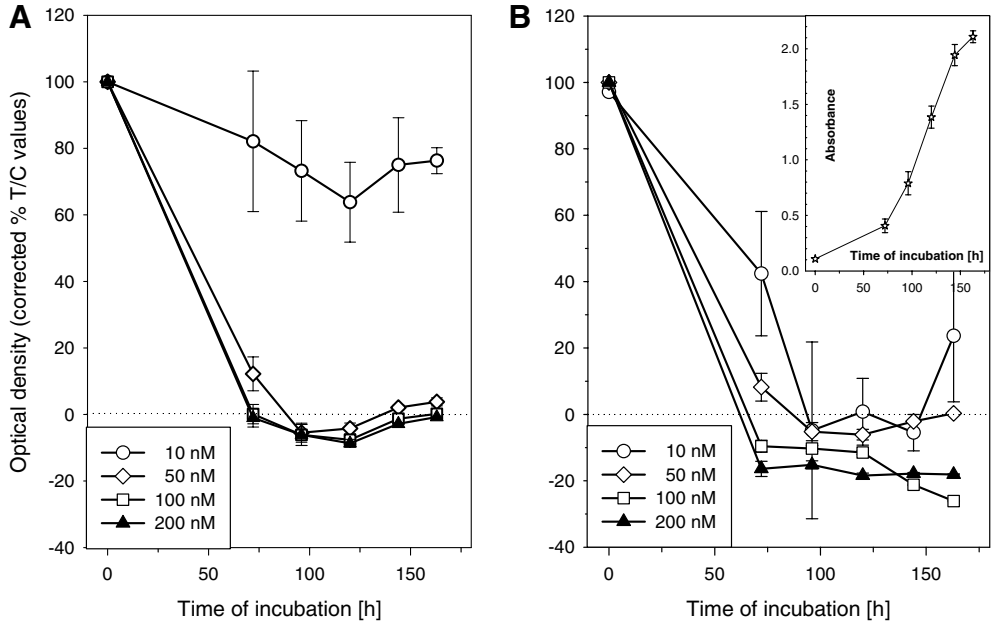

Figure 4. Proliferation of U-373 MG glioblastoma cells during permanent incubation with various concentrations of aroyl hydrazones **4e** (A) and **6a** (B). The growth of untreated control cells is shown on the insert.

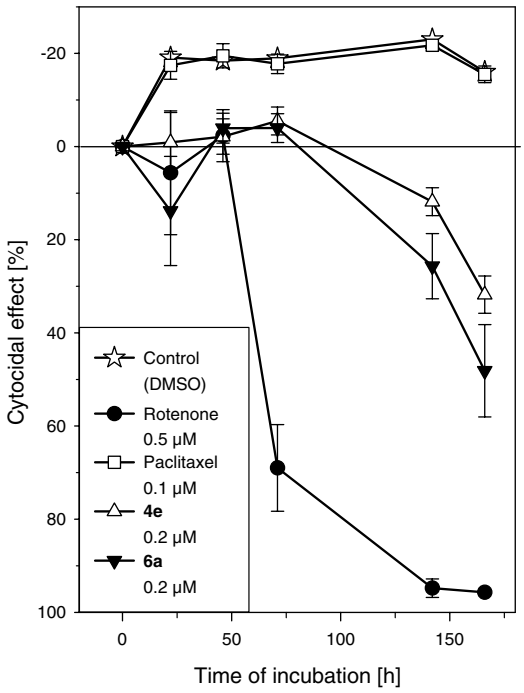

Figure 5. Incubation of resting U-373 MG glioblastoma cells with rotenone, paclitaxel, and hydrazones **4e** and **6a.**

the control cells. The chromosomes showed correct orientation and mitotic spindles were formed (Fig. 9C).

2.4. Activation of caspase-3

The inhibition of cell growth by the hydrazones **4a** and **6a** is accompanied by the occurrence of a substantial sub-G_1 fraction in the cell cycle analysis. This effect is probably due to apoptotic processes induced in G_1 and/or G_2 phase. The apoptotic path to cell death is characterized by the release of cytochrome *c* from the mitochondria, the induction of various caspase enzymes, condensation of the chromosomes, and the fragmentation of nuclear DNA.[9] In this study, the cleavage of the fluorogenic caspase-3 selective substrate, acetyl-DMQD-AMC, in HL-60 human leukemia cells was used as biochemical marker of apoptosis. In a preliminary experiment, one of the hydrazones (**5b**) was tested for its ability to increase caspase-3 and -9 activities within 24 h in HL-60 cells. It strongly enhanced the cleavage of the caspase-3 and -9 substrates when applied in a 1 µM concentration. In more detailed investigations, we studied the effect of four different hydrazones and of etoposide on the activation of caspase-3 at dose levels of 100 nM which is close to the IC_{50} values, and 500 nM which is two to fourfold higher than the IC_{90} values in this cell line (Table 3). At 100 nM, only compound **6a** induced caspase activity significantly while at 500 nM all compounds except **7a** and etoposide exerted a strong increase of caspase activity (Fig. 10). Obviously, the induction of caspase-3 parallels the antiproliferative effects because at 100 nM only derivative **6a** with the lowest IC_{50} value (50 nM; IC_{90}, 115 nM) was active, whereas at 500 nM all hydrazones except **7a** with the highest IC_{50} were active. As expected from the IC_{50} value (315 nM), etoposide was inactive at both concentrations. The differences between these two assays regarding the concentrations required for activity are probably due to the different periods of treatment (24 h for apoptosis studies vs 48 h for cytoxicities). These studies together with the flow cytometry data provide

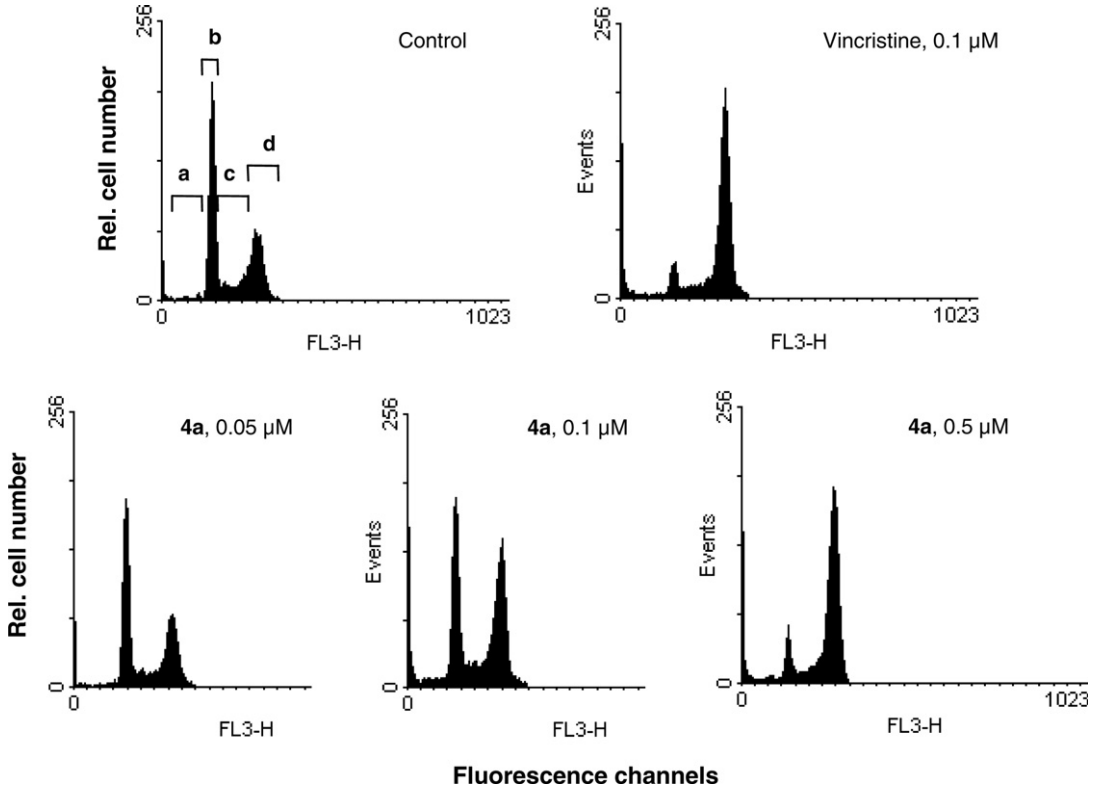

Figure 6. Flow cytometry analysis of cell cycle. MDA-MB 231 breast cancer cells were exposed to compound **4a** in various concentrations and vincristine for 24 h. The DNA content was quantified by the standard propidium iodide procedure, as described in Section 4. Cells are assigned to those in G_0/G_1- (label b), S- (label c), and G_2/M-phase (label d), and to sub-G_1 cells (label a), respectively, according to their DNA content.

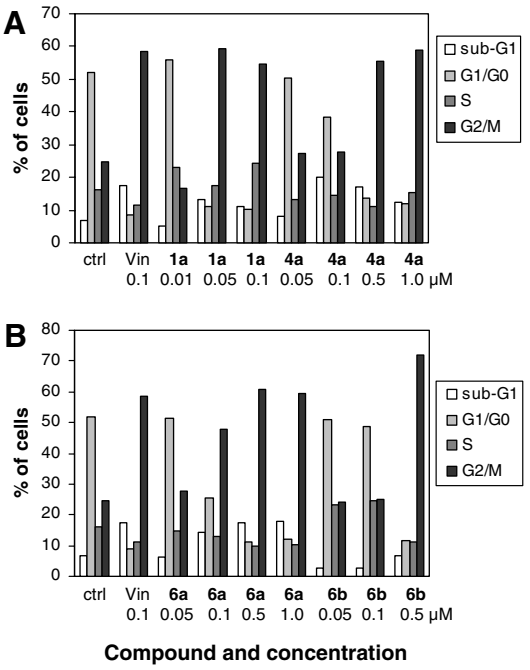

Figure 7. Cell cycle distribution of MDA-MB 231 cells treated for 24 h with 2-phenylindole-3-carbaldehyde **1a** and aroyl hydrazones **4a** (A), **6a**, and **6b** (B) in various concentrations. Vincristine (Vin) was used as reference drug. Percentages of sub-G_1 cells and cells in G_1/G_0-phase, S-phase, and G_2/M-phase are shown. Data refer to a representative experiment out of two.

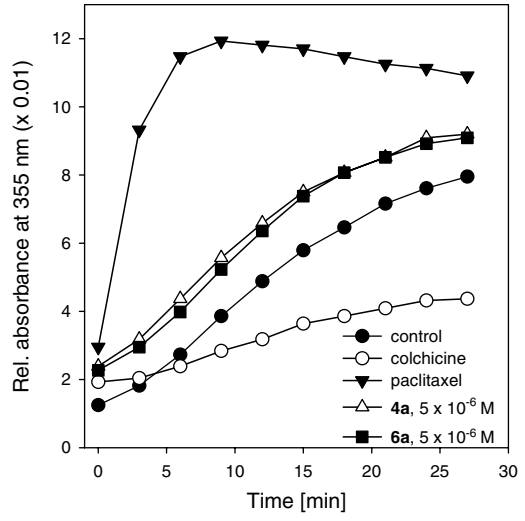

Figure 8. Effect of hydrazones **4a** and **6a**, paclitaxel (2 μM), and colchicine (5 μM) on tubulin assembly. Optical density at 355 nm was measured every minute over a period of 28 min simultaneously for all compounds and concentrations after temperature had been switched from 2 to 37 °C. Control wells contained tubulin and the solvent (0.1% DMSO).

strong evidence that apoptosis is the dominant mechanism of cell death for the title compounds.

2.5. Discussion

The objective of present and previous studies was the replacement of the carbonyl group in the 2-phenylindole-3-carbaldehyde structure **1** by new structural elements in order to avoid possible metabolic inactivation reactions and to increase the antimitotic potency of the 2-phenylindole pharmacophore. The results of this study showed that the aldehyde function can be converted to hydrazones by the reaction with aroyl hydrazine without abolishing the antiproliferative activity on cancer cells. Though the variation of substituents in the 2-phenyl ring was restricted to a small number of aldehydes, we could show that the influence of these substituents on the antitumor activity of the hydrazones is parallelled by analogous results in the aldehyde series. The similarity of the structure–activity relationships suggested a common mode of action for both aldehydes **1** and the corresponding hydrazones **5–7**. However, when we investigated the mode of action of the aroyl hydrazones we found that they must act through a different mechanism. The aldehydes **1** were shown to inhibit tubulin polymerization and this action was assumed to be responsible for the strong antimitotic effects of this class of compounds.[6] The corresponding aroyl hydrazones **4–7**, however, were unable of inhibiting tubulin polymerization, but blocked the cell cycle in G_2/M phase as the aldehydes did. This cell cycle arrest eventually leads to an apoptotic cell death as shown by the appearance of a substantial sub-G_1 fraction in the FACS analysis and the strong induction of caspase-3 activity at concentration close to the IC_{50} values.

The evidence of apoptotic processes, however, does not exclude a competing necrotic death of some of the cells.[7] The images of HL-60 cells obtained by light microscopy exhibited morphological changes typical for apoptotic processes following the treatment with the hydrazones at submicromolar concentrations (see Supplementary Material). When HL-60 cells were treated with 1.0 μM **5b** they showed similar morphologies to those treated with 8.0 μM etoposide after 24 h. It is interesting to note that a number of the HL-60 cells treated with compounds **4e**, **4i**, **6a**, and **7a** developed elongated structures and appear unable to divide (see Supplementary Material). This is consistent with the observation that the hydrazones block the cells at the G2/M interface.

Another interesting aspect of the hydrazones is their activity against quiescent cells as shown in the experiments with confluent U-373 MG glioblastoma cells. In this respect their antiproliferative profile differs from most other cytotoxic drugs.

From the data obtained in this study, the growth inhibitory effects of the indoles **4–7** can be rationalized as the result of an apoptotic cell death following the cell cycle arrest in G_2/M phase. However, the reason for the cell cycle blockade is not evident because the primary target of these indole derivatives is still unknown. The structure of the 2-phenylindole-based aroyl hydrazones is unique and does not resemble other compounds with antimitotic activity. There have been some hydrazones with antiproliferative activity described in the literature. Most of them are iron chelators such as **8**[10] or **9**[11] (Fig. 11) that derive from pyridoxal isonicotinoyl hydrazone and inhibit the enzyme ribonucleotide reductase, which is essential for cell growth. They usually arrest cells at the G_1/S interface. The aroyl hydrazones **4–7** of this study, however, are unlikely to form stable complexes with iron ions because they cannot form a six-membered chelate structure with the metal. When the cell cycle arrest in G_2/M phase is considered as the important criterion, other hydrazones such as the 2-benzimidazolyl hydrazones of 2-acetylpyridine[12] can also be excluded from the compounds with a related mode of action.

On the basis of the biological profile of the 2-phenylindole-based hydrazones other compounds were considered as potential analogues in respect with their biological action. Candidates are histone deacetylase inhibitors such as trichostatin A[13,14] or genistein[15] which both increase $p21^{WAF1/CIP1}$ expression, but they are only active at very high concentrations. An interesting compound in this respect is ellipticine (**10**, Fig. 11), a natural product with an indole substructure that inhibits the growth of MDA-MB 231 breast cancer cells. A variety of mechanisms have been dis-

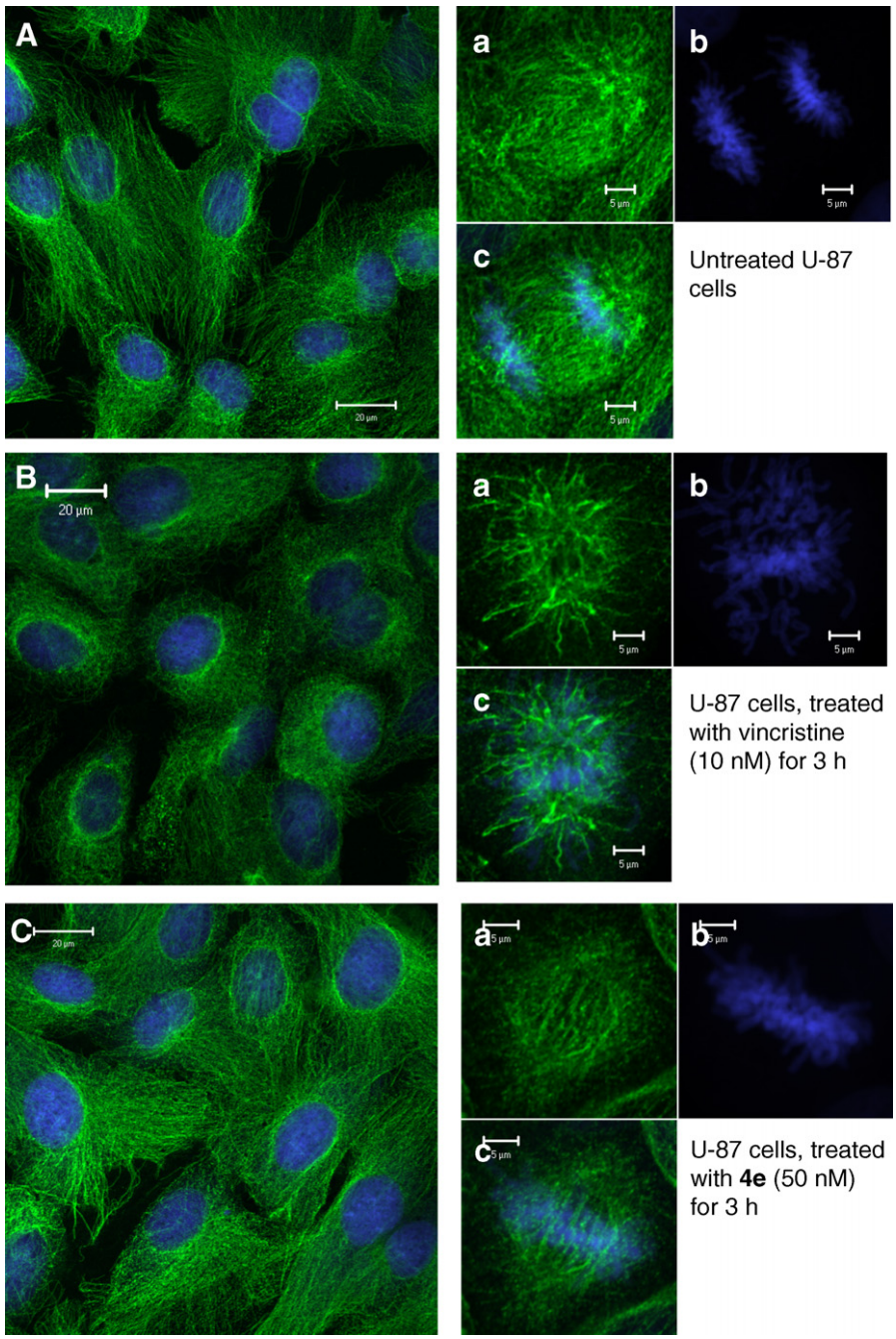

Figure 9. Effects of vincristine and hydrazone **4e** on the organization of cellular microtubule network and nuclear structure of U-87 MG human glioblastoma cells, visualized by confocal laser fluorescence microscopy. (A) Untreated control cells which undergo normal mitoses as shown in (a–c) ((a) stained tubulin; (b) stained nucleus; (c) merged images). (B) Vincristine (10 nM) leads to a disturbed and partially degraded tubulin network that has lost its function (a–c). (C) Hydrazone **4e** (50 nM) shows an unchanged microtubule network and normal mitotic spindles (a and c).

cussed as the reason for its antitumor activity including (i) DNA intercalation, (ii) inhibition of topoisomerase II, (iii) covalent alkylation of macromolecules, and (iv) induction of endoplasmic reticulum stress. Eventually all these actions lead to cell growth inhibition by cell cycle arrest in G_2/M phase and apoptosis by the activation of caspase-3 and -9.[16] It has been postulated that the cell cycle arrest occurs by reducing the activity of the Cdc2-cyclin B kinase complex due to down-regulation of multiple G_2/M regulating proteins.[16] Though the effect of ellipticine on the growth of MCF-7 breast cancer cells is nearly identical to that of MDA-MB 231 cells, significant differences in signal transduction pathways exist.[17] More recently, a carbazole sulfonamide **11** (Fig. 11) was discovered that exhibited a strong antimitotic effect on various tumor cell lines.[18] It also involves an arrest of the cell cycle in M-phase and induces apoptosis without inhibiting tubulin polymerization.

The lack of structural analogy of the 2-phenylindole-based aroyl hydrazones to known compounds with a similar biological profile makes it difficult to assign a definite molecular target to this class of compounds. Thus, further investigations are required to analyze cellular parameters controlling the cell cycle in cells treated with these 2-phenylindole derivatives.

Table 3
Antiproliferative activities of hydrazones **4e**, **4i**, **6a**, and **7a** on HL-60 human leukemia cells

Compound	IC_{50} ± SD[a] (nM)	IC_{90} ± SD[b] (nM)
4e	91 ± 21	164 ± 58
4i	74 ± 24	142 ± 40
6a	50 ± 16	115 ± 59
7a	213 ± 64	333 ± 129
Etoposide	315 ± 72	n.d.[c]

[a] 50% inhibition of cell growth after 48 h of treatment as determined by the MTT assay.
[b] 90% inhibition of cell growth after 48 h of treatment as determined by the MTT assay.
[c] Not determined.

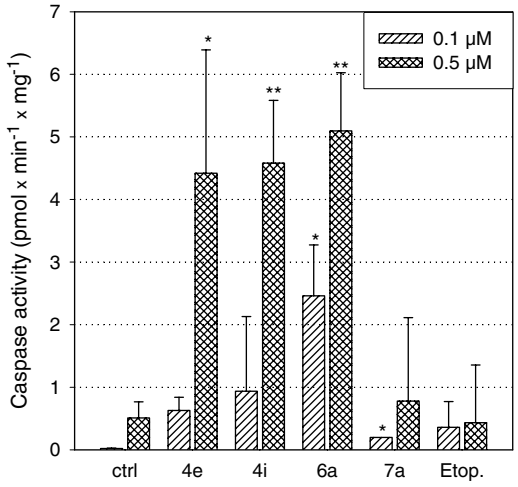

Figure 10. Effects of 100 and 500 nM of the aryl hydrazones **4e**, **4i**, **6a**, **7a**, and etoposide on caspase 3-like activity of HL-60 cells after a 24 h exposure. Controls show caspase activity of untreated HL-60 cells after 24 h. Bars represent means of three independent experiments ± SD. Single experiments are marked by an asterisk. The value for etoposide at 2.0 µM is 3.37 ± 0.78.

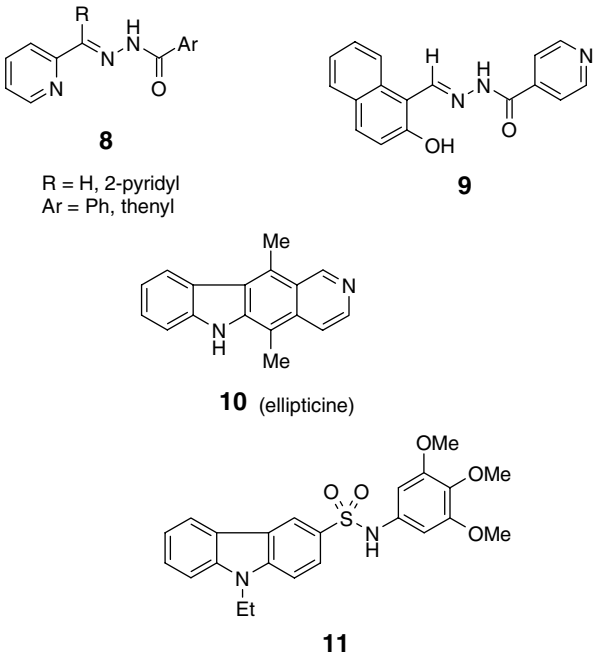

Figure 11. Examples for cytotoxic agents with an aroyl hydrazone structure (**8** and **9**), and of ellipticine (**10**) and the carbazole **11**. Compounds **8** and **9** act as iron chelators while ellipticine and compound **11** display biological profiles similar to that of the aroyl hydrazones **4–7**.

3. Conclusion

Four different 2-phenylindole-3-carbaldehydes **1a–d** which have previously been characterized as antimitotic agents of high potency were converted to the corresponding aroyl hydrazones **4–7** to render them stable to possible metabolic transformations of the aldehyde function and to explore the effect of nitrogen functionalities in 3-position. The in vitro assays on antiproliferative activity in human MDA-MB 231 and MCF-7 breast cancer cell lines revealed that the potencies of the 2-phenylindole-3-carbaldehydes decreased only by about one order of magnitude upon this structural modification. Interestingly, the structure of the aroyl group, benzoyl with various substituents in different positions, and nicotinoyl and isomers, had only a minor influence on the potency. Obviously, the (2-phenylindol-3-yl)methylene imine structure determines the antimitotic activity of these compounds.

Though the aroyl hydrazones share the same structure–activity relationships with the aldehydes, their molecular target(s) appear to be different because they do not interfere with the polymerization of tubulin, the dominant molecular action of the 2-phenylindole-3-carbaldehydes. Similar as the aldehydes, the aroyl hydrazones block the cell cycle in G_2/M phase and drive the tumor cells into apoptosis as demonstrated by the strong increase of caspase-3 activity by submicromolar concentrations. The question whether the necrotic cell death also plays a role cannot yet be clearly answered. Contrary to most other cytostatic agents the aroyl hydrazones of this study are also active against quiescent tumor cells as demonstrated in experiments with confluent U-373 MG glioblastoma cells. The biological characteristics of these new compounds make them interesting candidates for further development as anticancer agents.

4. Experimental

4.1. General methods

Melting points were determined on a Büchi 510 apparatus and are uncorrected. ^{1}H NMR spectra were recorded in DMSO-d_6 on AC-250, AVANCE300, and AVANCE400 spectrometers (Bruker) with TMS as internal standard and were in accord with the assigned structures. Mass spectra were obtained with a MAT SSQ 710A spectrometer (Finnigan). Purity of all compounds was checked by TLC. Elemental analyses were performed by the Mikroanalytisches Laboratorium, University of Regensburg. The syntheses of the starting aldehydes **1a**[5] and **1b–d**[6] have been described previously. The required carboxylic acid hydrazides were commercially available.

4.2. Preparation of 2-phenylindole-3-carbaldehyde aroyl hydrazones (4–7)

The 2-phenylindole-3-carbaldehydes **1a**, **1b**, **1c**, or **1d** (1 mmol), and the respective carboxylic acid hydrazide (1.2 mmol) were dissolved in EtOH (99%; 20 mL). After the addition of anhydrous acetic acid (4 mL), the mixture was heated under reflux for 1 h. Water was added to the hot reaction mixture until it turned opaque. On standing, the product precipitated and was recrystallized from EtOH.

4.2.1. Benzoic acid [[5-*n*-butyl-2-(4-methoxyphenyl)indol-3-yl] methylene]hydrazide (4a)

Light yellow solid (72% yield), mp 218 °C. ^{1}H NMR δ 0.93 (t, ^3J = 7.3 Hz, 3H, $-CH_2-CH_3$); 1.37 (sext, ^3J = 7.3 Hz, 2H, $-CH_2-CH_2-CH_3$); 1.63 (quin, ^3J = 7.5 Hz, 2H, $-CH_2-CH_2-CH_2-$); 2.70 (t,

^3J = 7.5 Hz, 2H, –CH_2–CH_2–); 3.85 (s, 3H, –OCH_3); 7.07 (dd, ^3J = 8.3 Hz, ^4J = 1.5 Hz, 1H, indole-H^6); 7.15, 7.92 (AA′BB′, ^3J = 8.5 Hz, 4H, phenyl-H); 7.33 (d, ^3J = 8.2 Hz, 1H, indole-H^7); 7.48–7.58 (m, 5H, benzoyl-H); 8.24 (s, 1H, indole-H^4); 8.71 (s, 1H, –CH=N); 11.50 (s, 1H, N–H); 11.68 (s, 1H, N–H). Anal. Calcd for $C_{27}H_{27}N_3O_2$: C, 76.21; H, 6.40; N, 9.87. Found: C, 75.48; H, 6.36; N, 9.61.

4.2.2. Benzoic acid [[5-*n*-butyl-2-[4-(trifluoromethyl)phenyl] indol-3-yl]methylene]hydrazide (4b)

Light yellow crystals (33% yield), mp 214–216 °C. ^{1}H NMR δ 0.94 (t, ^3J = 7.3 Hz, 3H, –CH_2–CH_3); 1.37 (sext, ^3J = 7.3 Hz, 2H, –CH_2–CH_2–CH_3); 1.63 (quin, ^3J = 7.6 Hz, 2H, –CH_2–CH_2–CH_2); 2.72 (t, ^3J = 7.6 Hz, 2H, –CH_2–CH_2); 7.14 (dd, ^3J = 8.3 Hz, ^4J = 1.5 Hz, 1H, indole-H^6); 7.39 (d, ^3J = 8.3 Hz, 1H, indole-H^7); 7.49–7.58 (m, 3H, benzoyl-H); 7.87, 7.96 (AA′BB′, ^3J = 8.3 Hz, 4H, phenyl-H); 7.90–7.94 (m, 2H, benzoyl-H); 8.28 (s, 1H, indole-H^4); 8.73 (s, 1H, –CH=N); 11.54 (s, 1H, N–H); 11.97 (s, 1H, N–H). Anal. Calcd for $C_{27}H_{24}F_3N_3O$: C, 69.97; H, 5.22; N, 9.07. Found: C, 69.70; H, 5.30; N, 8.62.

4.2.3. 4-Chlorobenzoic acid [[5-*n*-butyl-2-(4-methoxyphenyl) indol-3-yl]methylene]hydrazide (4c)

Light yellow crystals (63% yield), mp 223–226 °C. ^{1}H NMR δ 0.93 (t, ^3J = 7.3 Hz, 3H, –CH_2–CH_3); 1.36 (sext, ^3J = 7.3 Hz, 2H, –CH_2–CH_2–CH_3); 1.63 (quin, ^3J = 7.5 Hz, 2H, –CH_2–CH_2–CH_2); 2.70 (t, ^3J = 7.5 Hz, 2H, –CH_2–CH_2–); 3.85 (s, 3H, –OCH_3); 7.07 (dd, ^3J = 8.3 Hz, ^4J = 1.6 Hz, 1H, indole-H^6); 7.16, 7.95 (AA′BB′, ^3J = 8.7 Hz, 4H, phenyl-H); 7.33 (d, ^3J = 8.2 Hz, 1H, indole-H^7); 7.58 (m, 4H, benzoyl-H); 8.22 (s, 1H, indole-H^4); 8.69 (s, 1H, –CH=N); 11.54 (s, 1H, N–H); 11.68 (s, 1H, N–H). Anal. Calcd for $C_{27}H_{26}N_3O_2Cl$: C, 70.50; H, 5.70; N, 9.14. Found: C, 69.70; H, 5.54; N, 8.97.

4.2.4. 4-Chlorobenzoic acid [[5-*n*-butyl-2-[4-(trifluoromethyl) phenyl]indol-3-yl]methylene]hydrazide (4d)

Light yellow solid (69% yield), mp 218 °C. ^{1}H NMR δ 0.93 (t, ^3J = 7.3 Hz, 3H, –CH_2–CH_3); 1.37 (sext, ^3J = 7.4 Hz, 2H, –CH_2–CH_2–CH_3); 1.63 (quin, ^3J = 7.5 Hz, 2H, –CH_2–CH_2–CH_2–); 2.71 (t, ^3J = 7.5 Hz, 2H, –CH_2–CH_2); 7.14 (dd, ^3J = 8.3 Hz, ^4J = 1.5 Hz, 1H, indole-H^6); 7.39 (d, ^3J = 8.3 Hz, 1H, indole-H^7); 7.61, 7.95 (AA′BB′, ^3J = 8.6 Hz, 4H, phenyl-H); 7.93 (m, 4H, benzoyl-H); 8.26 (s, 1H, indole-H^4); 8.71 (s, 1H, –CH=N); 11.59 (s, 1H, N–H); 11,98 (s, 1H, N–H). Anal. Calcd for $C_{27}H_{23}F_3N_3OCl$: C, 65.13; H, 4.66; N, 8.44. Found: C, 64.89; H, 5.14; N, 7.50.

4.2.5. 4-Fluorobenzoic acid [[5-*n*-butyl-2-(4-methoxyphenyl) indol-3-yl]methylene]hydrazide (4e)

Brownish solid (37% yield), mp 210 °C. ^{1}H NMR δ 0.93 (t, ^3J = 7.4 Hz, 3H, –CH_2–C*H*$_3$); 1.37 (sext, ^3J = 7.4 Hz, 2H, –CH_2–C*H*$_2$–CH_3); 1.63 (quin, ^3J = 7.3 Hz, 2H, –CH_2–C*H*$_2$–CH_2–); 2.70 (t, ^3J = 7.5 Hz, 2H, –C*H*$_2$–CH_2–); 3.85 (s, 3H, –OCH_3); 7.07 (dd, ^3J = 8.2 Hz, ^4J = 1.6 Hz, 1H, indole-H^6); 7.16, 7.58 (AA′BB′, ^3J = 8.8 Hz, 4H, phenyl-H); 7.23–7.40 (m, 3H, phenyl-H, indole-H^7); 7.86–8.03 (m, 2H, phenyl-H); 8.22 (s, 1H, indole-H^4); 8.39, 8.69 (2s, 1H, –CH=N); 11.32, 11.49 (2s, 1H, N–H); 11.58; 11.67 (2s, 1H, N–H). Anal. Calcd for $C_{27}H_{26}FN_3O_2$: C, 73.12; H, 5.91; N, 9.47. Found: C, 73.18; H, 5.97; N, 9.44.

4.2.6. 4-Methoxybenzoic acid [[5-*n*-butyl-2-(4-methoxyphenyl) indol-3-yl]methylene]hydrazide (4f)

White crystals (71% yield), mp 226–228 °C. ^{1}H NMR δ 0.93 (t, ^3J = 7.3 Hz, 3H, –CH_2–CH_3); 1.36 (sext, ^3J = 7.4 Hz, 2H, –CH_2–CH_2–CH_3); 1.63 (quin, ^3J = 7.5 Hz, 2H, –CH_2–CH_2–CH_2–); 2.69 (t, ^3J = 7.6 Hz, 2H, –CH_2–CH_2–); 3.83 (s, 3H, –OCH_3); 3.85 (s, 3H, –OCH_3); 7.05, 7.16 (AA′BB′, ^3J = 8.8 Hz, 4H, phenyl-H); 7.06 (dd, ^3J = 6.8 Hz, ^4J = 1.6 Hz, 1H, indole-H^6); 7.32 (d, ^3J = 8.2 Hz, 1H, indole-H^7); 7.58, 7.91 (AA′BB′, ^3J = 8.7 Hz, 4H, benzoyl-H); 8.23 (s, 1H, indole-H^4); 8.69 (s, 1H, –CH=N); 11.38 (s, 1H, N–H); 11.65 (s, 1H, N–H). Anal. Calcd for $C_{28}H_{29}N_3O_3$: C, 73.82; H, 6.42; N, 9.22. Found: C, 73.10; H, 6.32; N, 9.10.

4.2.7. 4-Methoxybenzoic acid [[5-*n*-butyl-2-[4-(trifluoromethyl) phenyl]indol-3-yl]methylene]hydrazide (4g)

Light yellow solid (73% yield), mp 232 °C. ^{1}H NMR δ 0.93 (t, ^3J = 7.3 Hz, 3H, –CH_2–CH_3); 1.37 (sext, ^3J = 7.4 Hz, 2H, –CH_2–CH_2–CH_3); 1.63 (quin, ^3J = 7.5 Hz, 2H, –CH_2–CH_2–CH_2–); 2.71 (t, ^3J = 7.4 Hz, 2H, –CH_2–CH_2–); 3.83 (s, 3H, –OCH_3); 7.06, 7.91 (AA′BB′, ^3J = 8.8 Hz, 4H, phenyl-H); 7.13 (dd, ^3J = 8.3 Hz, ^4J = 1.4 Hz, 1H, indole-H^6); 7.39 (d, ^3J = 8.2 Hz, 1H, indole-H^7); 7.91 (m, 4H, benzoyl-H); 8.28 (s, 1H, indole-H^4); 8.72 (s, 1H, –CH=N); 11.42 (s, 1H, N–H); 11.94 (s, 1H, N–H). Anal. Calcd for $C_{28}H_{26}F_3N_3O_2$: C, 68.14; H, 5.31; N, 8.51. Found: C, 67.54; H, 5.42; N, 8.07.

4.2.8. 3-Methoxybenzoic acid [[5-*n*-butyl-2-(4-methoxyphenyl) indol-3-yl]methylene]hydrazide (4h)

Light yellow solid (65% yield), mp 213 °C. ^{1}H NMR δ 0.93 (t, ^3J = 7.4 Hz, 3H, –CH_2–C*H*$_3$); 1.37 (sext, ^3J = 7.4 Hz, 2H, –CH_2–C*H*$_2$–CH_3); 1.63 (quin, ^3J = 7.7 Hz, 2H, –CH_2–C*H*$_2$–CH_2–); 2.70 (t, ^3J = 7.7 Hz, 2H, –C*H*$_2$–CH_2–); 3.83 (s, 3H, –OCH_3); 3.85 (s, 3H, –OCH_3); 7.07 (dd, ^3J = 8.2 Hz, ^4J = 1.6 Hz, 1H, indole-H^6); 7.15, 7.59 (AA′BB′, ^3J = 8.8 Hz, 4H, phenyl-H); 7.33 (d, ^3J = 8.2 Hz, 1H, indole-H^7); 7.46 (m, 4H, phenyl-H); 8.24 (s, 1H, indole-H^4); 8.71 (s, 1H, –CH=N); 11.45 (s, 1H, N–H); 11.66 (s, 1H, N–H). Anal. Calcd for $C_{28}H_{29}N_3O_3$: C, 73.82; H, 6.42; N, 9.22. Found: C, 73.69; H, 6.36; N, 9.13.

4.2.9. 2-Methoxybenzoic acid [[5-*n*-butyl-2-(4-methoxyphenyl) indol-3-yl]methylene]hydrazide (4i)

Light yellow solid (60% yield), mp 179 °C. ^{1}H NMR *δ 0.87–0.97 (m, 3H,* –CH_2–C*H*$_3$); 1.22–1.44 (m, 2H, –CH_2–C*H*$_2$–CH_3); 1.63 (quin, ^3J = 7.4 Hz, 2H, –CH_2–C*H*$_2$–CH_2–); 2.38, 2.70 (t, ^3J = 8.0 Hz, 2H, –C*H*$_2$–CH_2–); 3.71, 3.86 (m, 6H, OCH_3); 6.90, 7.28 (2dd, ^3J = 8.2/ 7.4 Hz, ^4J = 1.6 Hz, 1H, indole-H^6); 7.03, 7.20 (2d, ^3J = 8.2/ 7.4 Hz, indole-H^7); 7.12, 7.56 (AA′BB′, ^3J = 8.8 Hz, 4H, phenyl-H); 7.05–7.15 (m, 2H, phenyl-H); 7.30–7.58 (m, 2H, phenyl-H); 8.21, 7.41–7.58 (s + m, 1H, indole-H^4); 8.29, 8.54 (2s, 1H, –CH=N); 11.17, 11.22 (s, 1H, N–H); 11.47, 11.65 (s, 1H, N–H). Anal. Calcd for $C_{28}H_{29}N_3O_3$: C, 73.82; H, 6.42; N, 9.22. Found: C, 73.07; H, 6.37; N, 8.93.

4.2.10. 4-Nitrobenzoic acid [[5-*n*-butyl-2-(4-methoxyphenyl) indol-3-yl]methylene]hydrazide (4j)

Brownish solid (87% yield), mp 233 °C (dec). ^{1}H NMR δ 0.79, 0.93 (t, ^3J = 7.3 Hz, 3H, –CH_2–CH_3); 1.37 (sext, ^3J = 7.3 Hz, 2H, –CH_2–CH_2–CH_3); 1.63 (quin, ^3J = 7.5 Hz, 2H, –CH_2–CH_2–CH_2–); 2.37, 2.70 (t, ^3J = 7.6 Hz, 2H, –CH_2–CH_2–); 3.85 (s, 3H, –OCH_3); 6.94, 7.08 (dd, ^3J = 8.2 Hz, ^4J = 1.5 Hz, 1H, indole-H^6); 7.16, 7.59 (AA′BB′, ^3J = 8.7 Hz, 4H, phenyl-H); 7.24, 7.34 (d, ^3J = 8.1 Hz, 1H, indole-H^7); 8.15–8.18 (m, 2H, benzoyl-H); 8.23 (s, 1H, indole-H^4); 8.36–8.39 (m, 2H, benzoyl-H); 8.71 (s, 1H, –CH=N); 11.74 (s, 1H, N–H); 11.77 (s, 1H, N–H). Anal. Calcd for $C_{27}H_{26}N_4O_4$: C, 68.92; H, 5.57; N, 11.91. Found: C, 68.57; H, 5.50; N, 11.92.

4.2.11. 4-Nitrobenzoic acid [[5-*n*-butyl-2-[4-(trifluoromethyl) phenyl]indol-3-yl]methylene]hydrazide (4k)

Orange solid (80% yield), dec > 235 °C. ^{1}H NMR δ 0.79, 0.94 (t, ^3J = 7.3 Hz, 3H, –CH_2–CH_3); 1.18, 1.37 (sext, ^3J = 7.3 Hz, 2H, –CH_2–CH_2–CH_3); 1.64 (quin, ^3J = 7.5 Hz, 2H, –CH_2–CH_2–CH_2); 2.38, 2.72 (t, ^3J = 7.5 Hz, 2H, –CH_2–CH_2–); 7.02, 7.15 (dd, ^3J = 8.3 Hz,

^4J = 1.5 Hz, 1H, indole-H^6); 7.31, 7.40 (d, ^3J = 8.3 Hz, 1H, indole-H^7); 7.88, 7.97 (AA′BB′, ^3J = 8.3 Hz, 4H, phenyl-H); 8.16, 8.38 (AA′BB′, ^3J = 8.8 Hz, 4H, benzoyl-H); 8.28 (s, 1H, indole-H^4); 8.73 (s, 1H, –CH=N); 11.65, 11.81 (s, 1H, N–H); 11.91, 12.03 (s, 1H, N–H). Anal. Calcd for $C_{27}H_{23}F_3N_4O_3$: C, 63.78; H, 4.56; N, 11.02. Found: C, 63.54; H, 4.54; N, 11.00.

4.2.12. 3-Hydroxybenzoic acid [[5-*n*-butyl-2-(4-methoxyphenyl) indol-3-yl]methylene]hydrazide (4l)

White solid (56% yield), mp 181 °C. ^{1}H NMR δ 0.93 (t, ^3J = 7.3 Hz, 3H, –CH_2–CH_3); 1.37 (sext, ^3J = 7.4 Hz, 2H, –CH_2–CH_2–CH_3); 1.63 (quin, ^3J = 7.5 Hz, 2H, –CH_2–CH_2–CH_2–); 2.70 (t, ^3J = 7.5 Hz, 2H, –CH_2–CH_2–); 3.85 (s, 3H, –OCH_3); 6.92–6.97 (m, 1H, phenyl-H); 7.06 (dd, ^3J = 8.2 Hz, ^4J = 1.6 Hz, 1H, indole-H^6); 7.15, 7.58 (AA′BB′, ^3J = 8.8 Hz, 4H, phenyl-H); 7.23–7.37 (m, 4H, phenyl-H, indole-H^7); 8.22 (s, 1H, indole-H^4); 8.70 (s, 1H, –CH=N); 9.72 (s, 1H, O–H); 11.40 (s, 1H, N–H); 11.65 (s, 1H, N–H). Anal. Calcd for $C_{27}H_{27}N_3O_3\cdot H_2O$: C, 70.57; H, 6.36; N, 9.14. Found: C, 70.40; H, 6.23; N, 9.02.

4.2.13. Pyridine-4-carboxylic acid [[5-*n*-butyl-2-(4-methoxyphenyl)indol-3-yl]methylene]hydrazide (5a)

Light yellow solid (79% yield), dec > 145 °C. ^{1}H NMR δ 0.93 (t, ^3J = 7 Hz, 3H, –CH_2–CH_3); 1.36 (sext, ^3J = 7 Hz, 2H, –CH_2–CH_2–CH_3); 1.63 (quin, ^3J = 7 Hz, 2H, –CH_2–CH_2–CH_2–); 2.70 (t, ^3J = 7 Hz, 2H, –CH_2–CH_2–); 3.85 (s, 3H, –OCH_3); 7.07 (dd, ^3J = 8 Hz, ^4J = 2 Hz, indole-H^6); 7.33, 7.58 (AA′BB′, ^3J = 9 Hz, 4H, phenyl-H); 7.33 (d, ^3J = 8 Hz, 1H, indole-H^7); 7.81, 8.77 (AA′BB′, ^3J = 6 Hz, 4H, pyridyl-H); 8.22 (s, 1H, indole-H^4); 8.70 (s, 1H, –CH=N); 11.67 (s, 1H, N–H). Anal. Calcd for $C_{26}H_{26}N_4O_2\cdot H_2O$: C, 70.25; H, 6.35; N, 12.60. Found: C, 70.68; H, 5.99; N, 12.69.

4.2.14. Pyridine-4-carboxylic acid [[5-*n*-butyl-2-[4-(trifluoromethyl)phenyl]indol-3-yl]methylene]hydrazide (5b)

Yellow powder (50% yield), mp 158–160 °C. ^{1}H NMR δ 0.93 (t, 3H, ^3J = 7 Hz, –CH_2–CH_3); 1.33 (m, 2H, –CH_2–CH_2–CH_3); 1.63 (m, 2H, –CH_2–CH_2–CH_2–); 2.71 (t, 2H, ^3J = 7 Hz, –CH_2–CH_2–); 7.13 (dd, 1H, ^3J = 8 Hz, ^4J = 2 Hz, indole-H^6); 7.39 (d, 1H, ^3J = 8 Hz, indole-H^7); 7.89 (m, 4H, phenyl-H); 8.26 (s, 1H, indole-H^4); 8.75 (m, 5H, pyridyl-H, –CH=N–); 11.73 (s, br, 1H, N–H); 12.02 (s, br, 1H, N–H). MS; *m*/*z* (%) 465 (100, $[MH]^+$); 463 (100, $[M-H]^-$). Anal. Calcd for $C_{26}H_{23}F_3N_4O\cdot H_2O$: C, 64.72; H, 5.22; N, 11.61. Found: C, 65.75; H, 4.92; N, 11.01.

4.2.15. Pyridine-4-carboxylic acid [[5-*n*-butyl-2-(4-ethylphenyl) indol-3-yl]methylene]hydrazide (5c)

Yellow powder (66% yield), mp 203–204 °C. ^{1}H NMR δ 0.93 (t, 3H, ^3J = 7 Hz, –CH_2–CH_3); 1.24 (t, ^3J = 7 Hz, –CH_2–CH_3); 1.36 (m, 2H, –CH_2–CH_2–CH_3); 1.63 (m, 2H, –CH_2–CH_2–CH_2–); 2.70 (m, 4H, –CH_2–CH_3 and –CH_2–CH_2–); 7.08 (dd, 1H, ^3J = 8 Hz, ^4J = 2 Hz, indole-H^6); 7.34 (d, 1H, ^3J = 8 Hz, indole-H^7); 7.43, 7.55 (AA′BB′, 4H, ^3J = 8 Hz, phenyl-H); 8.23 (s, 1H, indole-H^4); 8.72 (s, 1H, –CH=N); 7.83, 8.76 (AA′BB′, 4H, ^3J = 6 Hz, pyridyl-H); 11.70 (s, br, 1H, N–H); 11.77 (s, br, 1H, N–H). MS *m*/*z* (%) 425 (100, $[MH]^+$), 423 (100, $[M-H]^-$). Anal. Calcd for $C_{27}H_{28}N_4O\cdot H_2O$: C, 73.27; H, 6.83; N, 12.66. Found: C, 74.57; H, 6.77; N, 12.15.

4.2.16. Pyridine-4-carboxylic acid [[2-(4-methoxyphenyl)-5-methylindol-3-yl]methylene]hydrazide (5d)

Light green solid (84% yield), dec > 145 °C. ^{1}H NMR δ 2.45 (s, 3H, –CH_3); 3.85 (s, 3H, –OCH_3); 7.06 (d, ^3J = 8 Hz, 1H, indole-H^6); 7.15, 7.59 (AA′BB′, ^3J = 9 Hz, 4H, phenyl-H); 7.31 (d, ^3J = 8 Hz, 1H, indole-H^7); 8.22 (s, 1H, indole-H^4); 7.83, 8.76 (AA′BB′, ^3J = 6 Hz, 4H, pyridyl-H); 8.70 (s, 1H, –CH=N); 12.86 (s, br, 1H, N–H). Anal. Calcd for $C_{23}H_{20}N_4O_2$: C, 71.86; H, 5.24; N, 14.57. Found: C, 70.83; H, 4.97; N, 14.24.

4.2.17. Pyridine-3-carboxylic acid [[5-*n*-butyl-2-(4-methoxyphenyl)indol-3-yl]methylene]hydrazide (6a)

Yellow solid (65% yield), dec > 125 °C. ^{1}H NMR δ 0.93 (t, ^3J = 7.3 Hz, 3H, –CH_2–CH_3); 1.37 (sext, ^3J = 7.4 Hz, 2H, –CH_2–CH_2–CH_3); 1.63 (quin, ^3J = 7.5 Hz, 2H, –CH_2–CH_2–CH_2–); 2.70 (t, ^3J = 7.6 Hz, 2H, –CH_2–CH_2–); 3.86 (s, 3H, –OCH_3); 7.07 (dd, ^3J = 8.3 Hz, ^4J = 1.6 Hz, 1H, indole-H^6); 7.16, 7.58 (AA′BB′, ^3J = 8.8 Hz, 4H, phenyl-H); 7.33 (d, ^3J = 8.2 Hz, 1H, indole-H^7); 7.53 (m, 1H, pyridine-H^5); 8.23 (m, 1H, indole-H^4); 8.27 (m, 1H, pyridine-H^4); 8.69 (s, 1H, –CH=N–); 8.73 (m, 1H, pyridine-H^6); 9.07 (s, 1H, pyridine-H^2); 11.64 (s, 1H, N–H); 11.70 (s, 1H, N–H). Anal. Calcd for $C_{26}H_{26}N_4O_2\cdot H_2O$: C, 70.25; H, 6.35; N, 12.60. Found: C, 69.94; H, 5.80; N, 12.44.

4.2.18. Pyridine-3-carboxylic acid [[5-*n*-butyl-2-[4-(trifluoromethyl)phenyl]indol-3-yl]methylene]hydrazide (6b)

Light yellow solid (85% yield), mp 240–241 °C. ^{1}H NMR δ 0.94 (t, ^3J = 7.3 Hz, 3H, –CH_2–CH_3); 1.37 (sext,^3J = 7.5 Hz, 2H, –CH_2–CH_2–CH_3); 1.64 (quin, ^3J = 7.5 Hz, 2H, –CH_2–CH_2–CH_2–); 2.72 (t, ^3J = 7.5 Hz, 2H, –CH_2–CH_2–); 7.14 (dd, ^3J = 8.4 Hz, ^4J = 1.3 Hz, 1H, indole-H^6); 7.40 (d, ^3J = 8.2 Hz, 1H, indole-H^7); 7.57 (m, 1H, pyridine-H^5); 7.87, 7.96 (AA′BB′, ^3J = 8.4 Hz, 4H, phenyl-H); 8.24–8.44 (m, 2H, pyridine-H^4, indole-H^4); 8.71 (s, 1H, –CH=N–); 8.73–8.76 (m, 1H, pyridine-H^6); 9.08 (s, 1H, pyridine-H^2); 11.69 (s, 1H, N–H); 12.01 (s, 1H, N–H). MS: *m*/*z* (%): 465 (100, $[MH]^+$), 463 (100, $[M-H]^-$). Anal. Calcd for $C_{26}H_{23}F_3N_4O\cdot H_2O$: C, 64.72; H, 5.22; N, 11.61. Found: C, 64.69; H, 5.33; N, 10.95.

4.2.19. Pyridine-3-carboxylic acid [[5-*n*-butyl-2-(4-ethylphenyl)indol-3-yl]methylene]hydrazide (6c)

Yellow powder (30% yield), dec > 135 °C. ^{1}H NMR δ 0.93 (t, 3H, ^3J = 7 Hz, –CH_2–CH_3); 1.24 (t, ^3J = 7 Hz, –CH_2–CH_3); 1.36 (m, 2H, –CH_2–CH_2–CH_3); 1.63 (m, 2H, –CH_2–CH_2–CH_2–); 2.70 (m, 4H, –CH_2–CH_3 and –CH_2–CH_2–); 7.08 (dd, 1H, ^3J = 8 Hz, ^4J = 2 Hz, indole-H^6); 7.34 (d, 1H, ^3J = 8 Hz, indole-H^7); 7.48 (m, 5H, phenyl-H, pyridine-H^5); 8.26 (m, 2H, indole-H^4, pyridine-H^4); 8.71 (s, 1H, –CH=N); 8.73 (dd, 1H,^3J = 6 Hz, ^4J = 2 Hz, pyridine-H^6); 9.07 (d, 1H, ^4J = 2 Hz, pyridine-H^2); 11.64 (s, br, 1H, N–H); 11.74 (s, br, 1H, N–H). MS *m*/*z* (%) 425 (100, $[MH]^+$), 423 (100, $[M-H]^-$). Anal. Calcd for $C_{27}H_{28}N_4O\cdot H_2O$: C, 73.27; H, 6.83; N, 12.66. Found: C, 72.66; H, 6.67; N, 12.35.

4.2.20. Pyridine-2-carboxylic acid [[5-*n*-butyl-2-(4-methoxyphenyl)indol-3-yl]methylene]hydrazide (7a)

Light yellow solid (76% yield), mp 182–184 °C. ^{1}H NMR δ 0.94 (t, ^3J = 7.3 Hz, 3H, –CH_2–CH_3); 1.37 (sext, ^3J = 7.4 Hz, 2H, –CH_2–CH_2–CH_3); 1.64 (quin, ^3J = 7.5 Hz, 2H, –CH_2–CH_2–CH_2–); 2.70 (t, ^3J = 7.6 Hz, 2H, –C<u>H</u>$_2$–CH_2–); 3.86 (s, 3H, –OCH_3); 7.06 (dd, ^3J = 8.3 Hz, ^4J = 1.6 Hz, 1H, indole-H^6); 7.15, 7.62 (AA′BB′, ^3J = 8.8 Hz, 4H, phenyl-H); 7.33 (d, ^3J = 8.2 Hz, 1H, indole-H^7); 7.65 (m, 1H, pyridine-H^5); 8.05 (m, 1H, pyridine-H^4); 8.13 (m, 1H, pyridine-H^6); 8.27 (s, 1H, indole-H^4); 8.69 (m, 1H, pyridine-H^3); 8.89 (s, 1H, –CH=N–); 11.66 (s, 1H, N–H); 11.94 (s, 1H, N–H). Anal. Calcd for $C_{26}H_{26}N_4O_2$: C, 73.22; H, 6.14; N, 13.14. Found: C, 71.96; H, 5.72; N, 12.51.

4.2.21. Pyridine-2-carboxylic acid [[5-*n*-butyl-2-[4-(trifluoromethyl)phenyl]indol-3-yl]methylene]hydrazide (7b)

Yellow solid (71% yield), mp 204 °C. ^{1}H NMR δ 0.94 (t, ^3J = 7.3 Hz, 3H, –CH_2–CH_3); 1.37 (sext, ^3J = 7.4 Hz, 2H, –CH_2–CH_2–CH_3); 1.64 (quin, ^3J = 7.5 Hz, 2H, –CH_2–CH_2–CH_2–); 2.72 (t, ^3J = 7.6 Hz, 2H, –CH_2–CH_2–); 7.14 (dd, ^3J = 8.3 Hz, ^4J = 1.6 Hz, 1H, indole-H^6); 7.39 (d, ^3J = 8.3 Hz, 1H, indole-H^7); 7.65 (m, 1H, pyridine-H^5); 7.90, 7.95 (AA′BB′, ^3J = 8.8 Hz, 4H, phenyl-H); 8.06 (m, 1H, pyridine-H^4); 8.14 (m, 1H, pyridine-H^6); 8.32 (s, 1H, indole-H^4); 8.69 (m, 1H, pyridine-H^3); 8.96 (s, 1H, –CH=N–); 11.96 (s,

1H, N–H); 12.04 (s, 1H, N–H). Anal. Calcd $C_{26}H_{23}F_3N_4O$: C, 67.23; H, 4.99; N, 12.06. Found: C, 67.24; H, 4.94; N, 11.52.

4.3. Materials and reagents for bioassays

Drugs and biochemicals were obtained from Sigma (Deisenhofen, Germany) except where noted. All cell lines used (MDA-MB 231 and MCF-7 breast cancer cells, U-373 glioblastoma cells, and HL-60 leukemia cells) were of human origin, and were obtained from the American Type Culture collection (ATCC, Rockville, MD, USA).

4.4. Determination of antiproliferative activity

Hormone-independent human MDA-MB 231 breast cancer cells were grown in McCoy-5a medium, supplemented with L-glutamine (73 mg/L), gentamycin sulfate (50 mg/L), $NaHCO_3$ (2.2 g/L), and 5% sterilized fetal calf serum (FCS). At the start of the experiment, the cell suspension was transferred to 96-well microplates (100 μL/well). After the cells had grown for 2–3 days in a humidified incubator with 5% CO_2 at 37 °C, medium was replaced by one containing the test compounds (200 μL/well). Control wells (16/plate) contained 0.1% of DMF that was used for the preparation of stock solutions. Initial cell density was determined by addition of glutaric dialdehyde (1% in PBS; 100 μL/well) instead of test compound. After incubation for about 4 days, the medium was removed and 100 μL of glutaric dialdehyde in PBS (1%) was added for fixation. After 15 min, the solution of aldehyde was decanted. Cells were stained by treating them for 25 min with 100 μL of an aqueous solution of crystal violet (0.02%). After decanting, cells were washed several times with water to remove adherent dye. After addition of 100 μL EtOH (70%), plates were gently shaken for 2 h. Optical density of each well was measured in a microplate autoreader EL 309 (Bio-tek) at 578 nm.

For hormone-sensitive MCF-7 human breast cancer cells a similar procedure to that described for MDA-MB 231 cells was applied with modifications: Cells were grown in EMEM supplemented with sodium pyruvate (110 mg/L), gentamycin sulfate (50 mg/L), $NaHCO_3$ (2.2 g/L), phenol red, and 10% FCS.

U-373 MG glioblastoma/astrocytoma cells were cultivated under similar conditions as the MCF-7 cells except that the concentration of FCS was reduced to 5%. In the experiments with U-373 MG cells were fixed with glutaric dialdehyde after various times of incubation and stored in a refrigerator. At the end of the experiment, all plates were processed simultaneously. For the time–response curves drug effects were expressed as corrected T/C-values for each group according to the formula: $T/C = (T - C_0)/(C - C_0) \times 100$ (%), where T is the mean absorbance of treated cells, C the mean absorbance of untreated cells, and C_0 the mean absorbance of control cells at the time when the test compound was added.

4.5. Flow cytometry

MDA-MB 231 cells were grown to 70–80% confluence on the bottom of a 75 cm^2 culture flask. Test substances were dissolved in DMF and diluted to the required concentrations. The content of DMF in medium and in controls after 1000 times dilution was set to 0.1%. For each concentration one culture flask was used. Cells were exposed to test substances for 24 h. This incubation time was necessary to obtain a sufficient number of cells (5×10^6 cells). After incubation the cells were trypsinized, centrifuged (250*g*) in an excess of serum containing medium for 10 min, and washed with PBS.

The pellets of cells were resuspended in 1 mL of PBS and 9 mL of 70% EtOH (ice cold). EtOH and PBS were removed by centrifugation, and the cells were washed with PBS. After the addition of 0.5 mL of PBS and 0.5 mL of DNA extraction buffer, the cells were transferred into Eppendorf cups (2 mL), incubated for 5 min at room temperature, and centrifuged again. The cells are stained with 1 mL of propidium iodide solution for at least 30 min at room temperature and then analyzed by flow cytometry using a FACSCalibur™. For analysis, data files for four parameters were collected for 8000–15,000 events from each sample. The flow rate was adjusted to ca. 300 cells/s for appropriate accuracy. Data were analyzed by the WinMDI 2.8 software.

4.6. Tubulin polymerization assay on microplates

This assay was performed according to the vendor's protocol. Stock solutions of test compounds in DMSO were diluted 1:10 with G-PEM buffer. Ten microliters of this solution was added to the corresponding well of a microplate which was warmed in a microplate reader (Tecan) to 37 °C. Ice-cold tubulin was suspended in cold G-PEM buffer + glycerol (5%) and depolymerized at 0 °C within 1 min. Within 30 s, 100 μL of this solution was added to the warm solutions of the test compounds on the microplate and the plate returned to the reader. Absorbance at 355 nm was recorded at 37 °C for 30 min. Reference drugs were paclitaxel and colchicine; control wells contained only the solvent (1%).

4.7. Confocal laser scanning microscopy

U-87 MG cells were seeded into 8-well Lab-Tek Chamber Slides (Nunc, Wiesbaden, Germany). At 75% confluence the culture medium was replaced with medium containing vincristine (10 nM), hydrazone **4e** (50 nM), or the corresponding vehicle (EtOH). The cells were incubated at 37 °C for 3 h. After removal of the culture medium the cells were fixed with 4% paraformaldehyde solution in PBS for 20 min at room temperature. Thereafter each well was washed three times with PBS supplemented by 0.5% BSA. For permeabilization cells were incubated with PBS (+0.5% BSA) containing 1% Triton-X 100 (Serva, Heidelberg, Germany) for 10 min at room temperature, and washed three times with PBS (+0.5% BSA).

Nuclei and chromosomes were stained with SYTOXGreen® nucleic acid stain (Molecular Probes, Eugene, OR, USA). Microtubules were stained using mouse antihuman α-tubulin primary antibody (Dianova, Hamburg, Germany) and Cy5-conjugated goat anti-mouse secondary antibody (Molecular Probes). All antibodies were used in a 1:200 dilution in PBS, containing 0.5% BSA. A Carl Zeiss Axiovert 200 M LSM510 confocal laser scanning microscope was employed for acquisition of fluorescence images.

4.8. Caspase-3 activation studies

HL-60 human acute myeloid leukemia cells (DSMZ, Braunschweig, FRG) were maintained in logarithmic growth in RPMI 1640 supplemented with 10% FCS, 30 mg/L of penicillin G and 40 mg/L of streptomycin sulfate. For each experiment, apoptosis was induced by treatment of 3 million cells at 5×10^5 cells/mL with either an indole derivative or etoposide at either 100 or 500 μM. Cells were incubated in a humid atmosphere of 5% CO_2 at 37 °C and the cell lysates were prepared 24 h after treatment.

For the preparation of the cell-free extracts, all steps were performed at 0 °C. Cells were pelleted at 500g for 4 min, washed with PBS, once again pelleted at 500g for 4 min, and resuspended in hypotonic Hepes buffer (10 mM Hepes, pH 7.0; 5 mM D,L-dithiothreitol (DTT); 2 mM Na–EDTA; 0.1% (w/v) CHAPS). After a 20 min incubation on ice, lysates were centrifuged at 10,000g for 10 min. The supernatant was removed while taking care to avoid the pellet. Forty microliter of aliquots containing 3–7 μg of cytosolic protein (estimated by a modified Bradford method) were pre-incubated with 100 nM of the protease inhibitor benzyloxycarbonyl-Asp-Glu-Val-Asp-chloromethylketone (Bachem, Heidelberg, Germany). The samples were frozen at −32 °C. All experiments were performed within three weeks of extract preparation.

Caspase-3 activities were assessed by monitoring by HPLC the cleavage of a fluorochrome tagged synthetic substrates acetyl-Asp-Met-Gln-Asp-7-amino-4-methyl-coumarin (Ac-DMQD-AMC), synthesized as previously described.[19] After thawing of lysates, 3 μL of the substrate was added (final concentration of Ac-DMQD-AMC was 1.0 μM). The samples were incubated for 60 min at 30 °C. After this time, 20 μL of sample was injected directly into an RP-HPLC system (Merck-Hitachi) and the AMC was separated on a C18 column (Macherey-Nagel CC250/4 Nucleosil 120-5 C18) with a mobile phase of 1:1 acetonitrile/water containing 0.1% trifluoroacetic acid and set at a flow rate of 0.7 mL/min. Column temperature was 30°C. Retention time of AMC was 4.3 min. Quantification of AMC took place with a fluorescence detector (L-7485, Merck) that used an excitation wavelength of 355 or 400 nm and emission wavelength of 435 nm. Control experiments (data not shown) confirmed that the release of AMC was linear for at least 60 min at the conditions specified. AMC standards of 20–1500 fmol were used to construct a calibration curve so that the amounts of AMC released could be quantified.

To estimate the specific caspase activity, measurements of blank (substrate only), negative samples (substrate + cell lysate + inhibitor), and positive samples (substrate + cell lysate without inhibitor) were performed. The difference between the amount of AMC released in the positive and negative samples constituted the specific amount of AMC released by caspase-3. From each result obtained as fluorescence units (peak area), the blank values were subtracted. Thus, the final results are presented as amount of cleaved AMC (pmol/mg min) that can be suppressed by the selective caspase inhibitor benzyloxycarbonyl-Asp-Glu-Val-Asp-chloromethylketone.

Acknowledgments

The authors thank Dr. Dietmar Gross, University of Regensburg, for performing the confocal laser microscopy, and Renate Liebl and Susanne Bollwein for their excellent technical assistance.

Supplementary data

Supplementary data associated with this article can be found, in the online version, at doi:10.1016/j.bmc.2008.04.071.

References and notes

1. Biberger, C.; von Angerer, E. *J. Steroid Biochem. Mol. Biol.* **1996**, *58*, 31–43.
2. von Angerer, E.; Biberger, C.; Holler, E.; Koop, R.; Leichtl, S. *J. Steroid Biochem. Mol. Biol.* **1994**, *49*, 51–62.
3. Golob, T.; Liebl, R.; von Angerer, E. *Bioorg. Med. Chem.* **2002**, *10*, 3941–3953.
4. Walter, G.; Liebl, R.; von Angerer, E. *J. Steroid Biochem. Mol. Biol.* **2004**, *88*, 409–420.
5. Gastpar, R.; Goldbrunner, M.; Marko, D.; von Angerer, E. *J. Med. Chem.* **1998**, *41*, 4965–4972.
6. Kaufmann, D.; Pojarova, M.; Vogel, S.; Liebl, R.; Gastpar, R.; Gross, D.; Nishino, T.; Pfaller, T.; von Angerer, E. *Bioorg. Med. Chem.* **2007**, *15*, 5122–5136.
7. Pojarova, M.; Kaufmann, D.; Gastpar, R.; Nishino, T.; Reszka, P.; Bednarski, P. J.; von Angerer, E. *Bioorg. Med. Chem.* **2007**, *15*, 7368–7379.
8. Vibet, S.; Maheo, K.; Gore, J.; Dubois, P.; Bougnoux, P.; Chourpa, I. *Drug Metab. Dispos.* **2007**, *35*, 822–828.
9. Chang, H. Y.; Yang, X. *Microbiol. Mol. Biol. Rev.* **2000**, *64*, 821–846.
10. Whitnall, M.; Howard, J.; Ponka, P.; Richardson, D. R. *Proc. Natl. Acad. Sci. U.S.A.* **2006**, *103*, 14901–14906.
11. Green, D. A.; Antholine, W. E.; Wong, S. J.; Richardson, D. R.; Chitambar, C. R. *Clin. Cancer Res.* **2001**, *7*, 3574–3579.
12. Easmon, J.; Puerstinger, G.; Roth, T.; Fiebig, H. H.; Jenny, M.; Jaeger, W.; Heinisch, G.; Hofmann, J. *Int. J. Cancer* **2001**, *94*, 89–96.
13. Herold, C.; Ganslmayer, M.; Ocker, M.; Hermann, M.; Geerts, A.; Hahn, E. G.; Schuppan, D. *J. Hepatol.* **2002**, *36*, 233–240.
14. Wetzel, M.; Premkumar, D. R.; Arnold, B.; Pollack, I. F. *J. Neurosurg.* **2005**, *103*, 549–556.
15. Shao, Z. M.; Alpaugh, M. L.; Fontana, J. A.; Barsky, S. H. *J. Cell Biochem.* **1998**, *69*, 44–54.
16. Kuo, P. L.; Hsu, Y. L.; Kuo, Y. C.; Chang, C. H.; Lin, C. C. *Anticancer Drugs* **2005**, *16*, 789–795.
17. Kuo, P. L.; Hsu, Y. L.; Chang, C. H.; Lin, C. C. *Cancer Lett.* **2005**, *223*, 293–301.
18. Hu, L.; Li, Z. R.; Li, Y.; Qu, J.; Ling, Y. H.; Jiang, J. D.; Boykin, D. W. *J. Med. Chem.* **2006**, *49*, 6273–6282.
19. Rezska, P.; Methling, K.; Lalk, M.; Xiao, Z.; Weisz, K.; Bednarski, P. J. *Tetrahedron Asymm.* **2008**, *19*, 49–59.